

# Effect of Friction Stir Processing Procedures on Microstructure and Mechanical Properties of Mg-Al-Zn Casting

A.H. FENG, B.L. XIAO, Z.Y. MA, and R.S. CHEN

Cast Mg-Al-Zn (AZ80) alloy was subjected to friction stir processing (FSP) with three different FSP procedures: single pass, single pass with a pre-solution treatment (pre-ST), and two pass. FSP resulted in remarkable grain refinement, significant breakup, and dissolution of the coarse, networklike  $Mg_{17}Al_{12}$  phase. While the single-pass FSP procedure produced a heterogeneous microstructure with  $Mg_{17}Al_{12}$  particle-rich bands, both the pre-ST FSP and the two-pass FSP procedures resulted in the generation of a uniform microstructure. The pre-ST FSP and two-pass FSP samples exhibited significantly enhanced strength and ductility due to remarkable grain refinement and dissolution of coarse  $Mg_{17}Al_{12}$  phase. A post-FSP aging resulted in the precipitation of fine  $Mg_{17}Al_{12}$  particle, thereby increasing the strength of the FSP samples. Among three FSP samples, the aged two-pass FSP sample exhibited the highest ultimate tensile strength (UTS) of 356 MPa and an elongation of 17 pct.

DOI: 10.1007/s11661-009-9923-0

© The Minerals, Metals & Materials Society and ASM International 2009

## I. INTRODUCTION

MAGNESIUM alloys with low density, high thermal conductivity, good damping characteristics, and high specific strength are one of the lightest metals used for structural applications.<sup>[1]</sup> However, the use of the magnesium alloys has been strongly limited because of their low ductility resulting from the limited number of independent slip systems in hexagonal-close-packed (hcp) structure.<sup>[2]</sup> Grain refinement is an effective method to enhance the mechanical properties of the magnesium alloys. The correlation between the grain size and mechanical properties of the magnesium alloys based on the Hall-Petch relation has been well documented.<sup>[3,4]</sup>

Generally, commercial cast magnesium alloys fall into two classes: the Mg-Al-Zn (AZ) and Mg-Al-Mn (AM) systems, developed for room-temperature strength and ductility; and the Mg-Al-RE (AE) and Mg-Al-Si (AS) systems, developed for improved elevated-temperature performance.<sup>[5]</sup> For the AZ magnesium alloys, no reliable grain refining additive exists due to the interaction between impurity elements (such as zirconium) and aluminum, thereby resulting in poor grain refinement.<sup>[6,7]</sup> Therefore, the as-cast AZ magnesium alloys with higher aluminum content such as AZ91 and AZ80

alloys exhibit low strength and ductility due to the coarse grains and the presence of the coarse network-like grain boundary phase  $\beta$ - $Mg_{17}Al_{12}$ . It is necessary to modify the distribution and morphology of the  $\beta$ - $Mg_{17}Al_{12}$  phase and refine the matrix grains to enhance the mechanical properties of the AZ magnesium castings.

Two approaches have been used for this purpose. The first is the heat-treatment procedure. Conventionally, a solution treatment at a higher temperature of  $\sim 413$  °C was used to dissolve the coarse eutectic  $Mg_{17}Al_{12}$  network into the magnesium matrix. After the solution treatment, an artificial aging resulted in the reprecipitation of fine  $Mg_{17}Al_{12}$  particles, thereby improving the mechanical properties of the AZ magnesium alloys. However, for the AZ magnesium alloys, it takes up to  $\sim 40$  hours to achieve the complete dissolution of the eutectic  $\beta$ - $Mg_{17}Al_{12}$  phase due to the low diffusion rate of aluminum in the magnesium matrix.<sup>[8]</sup> Therefore, the conventional T6 procedure is not only time-consuming, resulting in increased material cost, but also causes severe surfacial oxidation and remarkable grain growth. Recently, an improved heat treatment  $T_x$  ( $\sim 370$  °C for 1 to 2 hours) was developed, which resulted in an improved combination of strength and ductility due to the modification of the distribution and morphology of the coarse eutectic  $Mg_{17}Al_{12}$  network.<sup>[9]</sup> The second is the plastic working procedure. It was reported that various processing techniques, such as thermomechanical processing and equal channel angular pressing, can improve the ductility and strength of the cast magnesium alloys significantly due to the refinement of both  $\beta$ - $Mg_{17}Al_{12}$  phase and grains.<sup>[10]</sup>

Friction stir processing (FSP), a development based on the basic principle of friction stir welding (FSW),<sup>[11,12]</sup> has currently attracted extensive attention for producing fine-grained microstructures<sup>[13,14]</sup> and surface composites<sup>[15]</sup>

A.H. FENG, Research Fellow, formerly with the Institute of Metal Research, Chinese Academy of Sciences, is with the Department of Mechanical and Industrial Engineering, Ryerson University, Toronto, ON M5B 2K3, Canada. B.L. XIAO, Associate Professor, and Z.Y. MA, Professor, Shenyang National Laboratory for Materials Science, and R.S. CHEN, Professor, are with the Institute of Metal Research, Chinese Academy of Sciences, Shenyang 110016, P.R. China. Contact e-mail: zyma@imr.ac.cn

Manuscript submitted January 23, 2009.

Article published online August 14, 2009

and for modifying the microstructure of heterogeneous metallic materials.<sup>[16,17]</sup> Especially, FSP of the as-cast alloys resulted in extensive grain refinement, breakup, and dissolution of the coarse second-phase particles, and closure of the porosity, thereby offering attractive strength and ductility.<sup>[16,17]</sup> Recently, research into FSP magnesium-based alloys has demonstrated that effective microstructural homogenization and refinement can be achieved as a result of severe plastic deformation and dynamic recrystallization.<sup>[3,4,18–24]</sup>

Our previous work has indicated that two-pass FSP combined with subsequent aging is a simple and effective approach to enhance the mechanical properties of AZ91D casting.<sup>[18]</sup> Furthermore, a preliminary comparative study indicated that single-pass FSP on AZ91D casting produced a heterogenous microstructure with low strength and ductility; however, a pre-solution treatment (pre-ST) prior to FSP resulted in improved microstructural uniformity and mechanical properties.<sup>[16]</sup> In this study, as-cast AZ80, a high-strength wrought magnesium alloy with composition similar to that of AZ91D, was subjected to FSP with three different FSP procedures: single pass, single pass with a pre-ST, and two pass. The microstructural evolution during FSP and post-FSP aging was examined and the mechanical properties of the FSP samples were evaluated. The aim is to (1) identify the optimized FSP procedure for the AZ magnesium alloy modification and (2) examine the possibility of using the FSP procedure to replace the conventional T6-solution heat treatment for the magnesium alloys.

## II. EXPERIMENTAL

As-cast AZ80 alloy billet with a composition of 8.5Al-0.5Zn-0.12Mn (wt pct) was used in this study. Eight-millimeter-thick plates were machined from the billet and subjected to FSP at a tool rotation rate of 400 rpm and a traverse speed of 100 mm/min. A steel tool with a shoulder 24 mm in diameter and a threaded cylindrical pin 8 mm in diameter and 6 mm in length was used. Three FSP procedures were used in this work. The first is single-pass FSP. The second is single-pass FSP with a pre-ST at 415 °C for 16 hours (hereafter referred to as the pre-ST FSP sample). The third is two-pass FSP with a 100 pct overlap and the same forward directions (hereafter referred to as the two-pass FSP sample). After FSP, part of the FSP samples were subjected to aging (177 °C/10 h).

The specimens for microstructural examinations were cross sectioned perpendicular to the FSP direction. Microstructural characterization and analysis were carried out by optical microscopy (OM), scanning electron microscopy (SEM, Hitachi\* S-3400 N), and differential

---

\*Hitachi is a trademark of Hitachi High-Technologies Corporation, Tokyo, Japan.

scanning calorimetry (DSC, Q1000V9.4 Build287). The

specimens for OM and SEM were prepared by mechanical polishing and etching using a solution of 3 g picric acid + 20 mL acetic acid + 50 mL ethanol + 20 mL water. Grain sizes were estimated by the linear intercept method. The crystal lattice parameters were determined by theta and 2-theta step scanning methods using an X-ray diffractometer. The Vickers hardness measurement was performed on a LECO-LM-247AT\*\* machine

---

\*\*LECO is a trademark of LECO Corporation, St. Joseph, MI.

along the midthickness of the stir zone (SZ) by applying 200-g load for 10 seconds.

Tensile specimens with a gage length of 10 mm, a width of 2 mm, and a thickness of 1.6 mm were machined parallel to the FSP direction with the gage being completely within the SZ. Tensile tests were carried out at an initial strain rate of  $1 \times 10^{-3} \text{ s}^{-1}$  in an Instron<sup>†</sup>

---

<sup>†</sup>Instron is a trademark of Instron Corporation, Norwood, MA.

5848 microtester. The fracture surfaces were examined on a scanning electron microscope (Hitachi S-3400 N).

## III. RESULTS

The as-received AZ80 base metal (BM) exhibited a typical cast microstructure, characterized by the coarse eutectic  $\text{Mg}_{17}\text{Al}_{12}$  network distributed at the grain boundaries, with the average grain size being  $\sim 280 \mu\text{m}$  (Figure 1(a)). Solution treatment at 415 °C for 16 hours resulted in fundamental dissolution of the coarse eutectic  $\text{Mg}_{17}\text{Al}_{12}$  phase into the matrix (Figure 1(b)), thereby producing a supersaturated solid solution. Only a few  $\text{Mg}_{17}\text{Al}_{12}$  particles were occasionally found at the grain triple junctions, as shown by a black arrow in Figure 1(b). However, the grains were significantly coarsened ( $\sim 420 \mu\text{m}$ ) after the solution treatment. In the single-pass FSP sample, the microstructure was obviously heterogeneous with a distinctly visible strip-like structure (Figure 1(c)), and the striplike structure appeared to be associated with the fine particles (Figure 1(d)). By comparison, the pre-ST FSP sample was characterized by fine and uniform recrystallized grains with an average grain size of  $14.6 \mu\text{m}$  (Figure 1(e)). Similarly, fine and uniform grain structure was observed in the two-pass FSP sample with an average grain size of  $10.5 \mu\text{m}$  (Figure 1(f)).

The SEM examinations indicated that the striplike structure in the single-pass FSP sample was associated with the finer grains and particle-rich bands (Figure 2(a)). The particles in the particle-rich bands were determined to be the  $\text{Mg}_{17}\text{Al}_{12}$  phase by energy-dispersive spectroscopy (EDS) analyses. In the regions with uniform grained structure in the single-pass FSP sample (Figure 2(b)), EDS analyses indicated that the grain interior contained 6.2 wt pct Al. The pre-ST and two-pass FSP samples were characterized by fine and

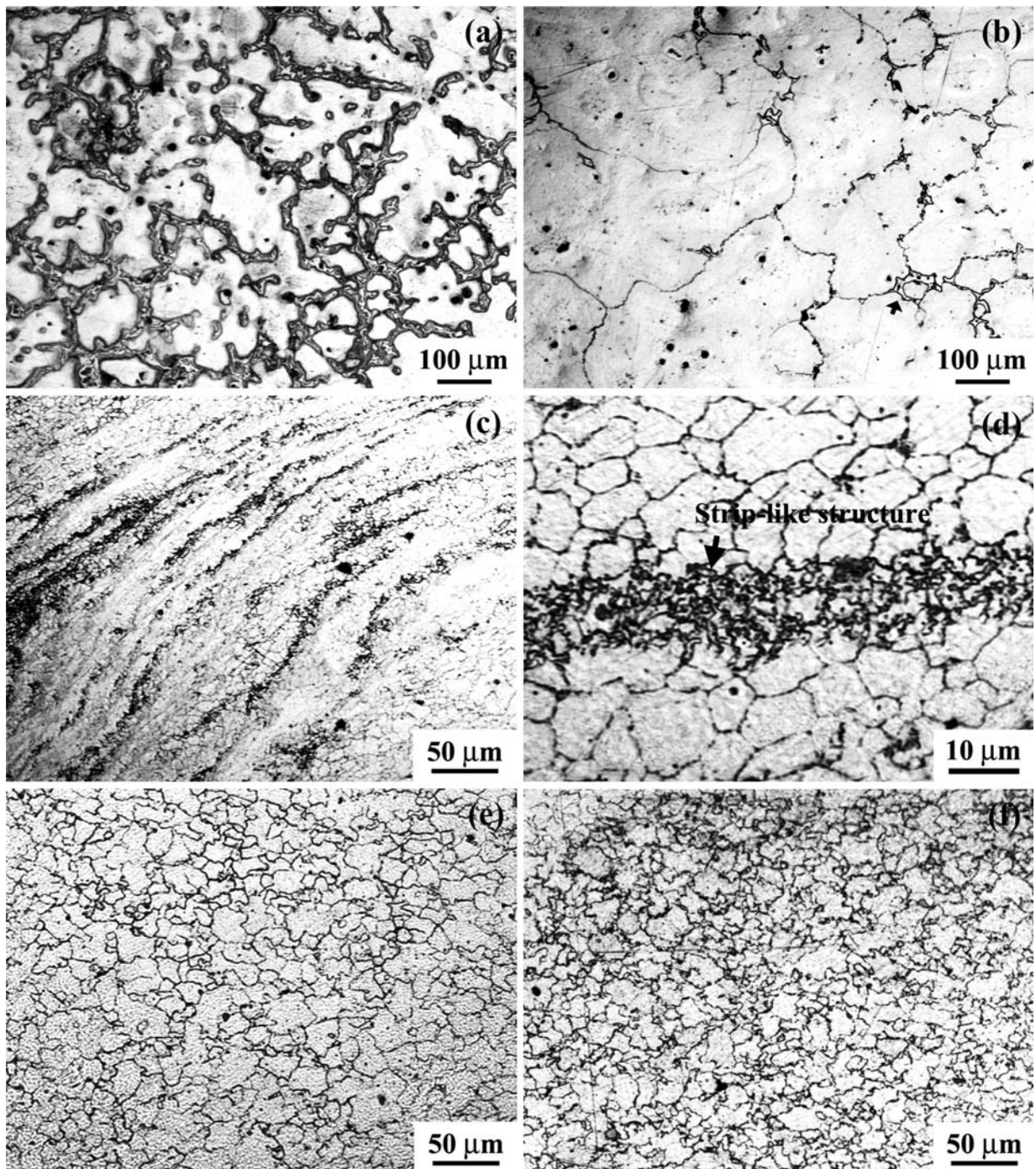


Fig. 1—Optical microstructure of AZ80 samples: (a) as-cast, (b) cast + solution, (c) and (d) single-pass FSP, (e) pre-ST FSP, and (f) two-pass FSP.

uniform grains, and no  $\beta$ - $Mg_{17}Al_{12}$  phase was detected within the grains under a scanning electron microscope (Figures 2(c) and (d)). The EDS analyses revealed that the grain interior contained 6.3 and 7.1 wt pct Al for the pre-ST and two-pass FSP samples, respectively, indicating that more aluminum was dissolved into the magnesium matrix for the two-pass FSP sample. Furthermore, for all the FSP samples, EDS analyses revealed a higher Al content of larger than 8.5 wt pct at the grain boundaries, indicating that there were fine  $Mg_{17}Al_{12}$

phase particles distributed at the grain boundaries, as shown by Figures 2(b) through (d).

The crystal lattice parameters of the pre-ST and two-pass FSP samples are shown in Table 1. Compared to those of pure magnesium, the crystal lattice parameters of the as-FSP AZ80 samples exhibited a remarkable shrinkage with a slight increase in the ratio of  $c$ -axis to  $a$ -axis. Figure 3 shows the relationship between the crystal lattice parameters and the aluminum concentration in the magnesium matrix determined by EDS.

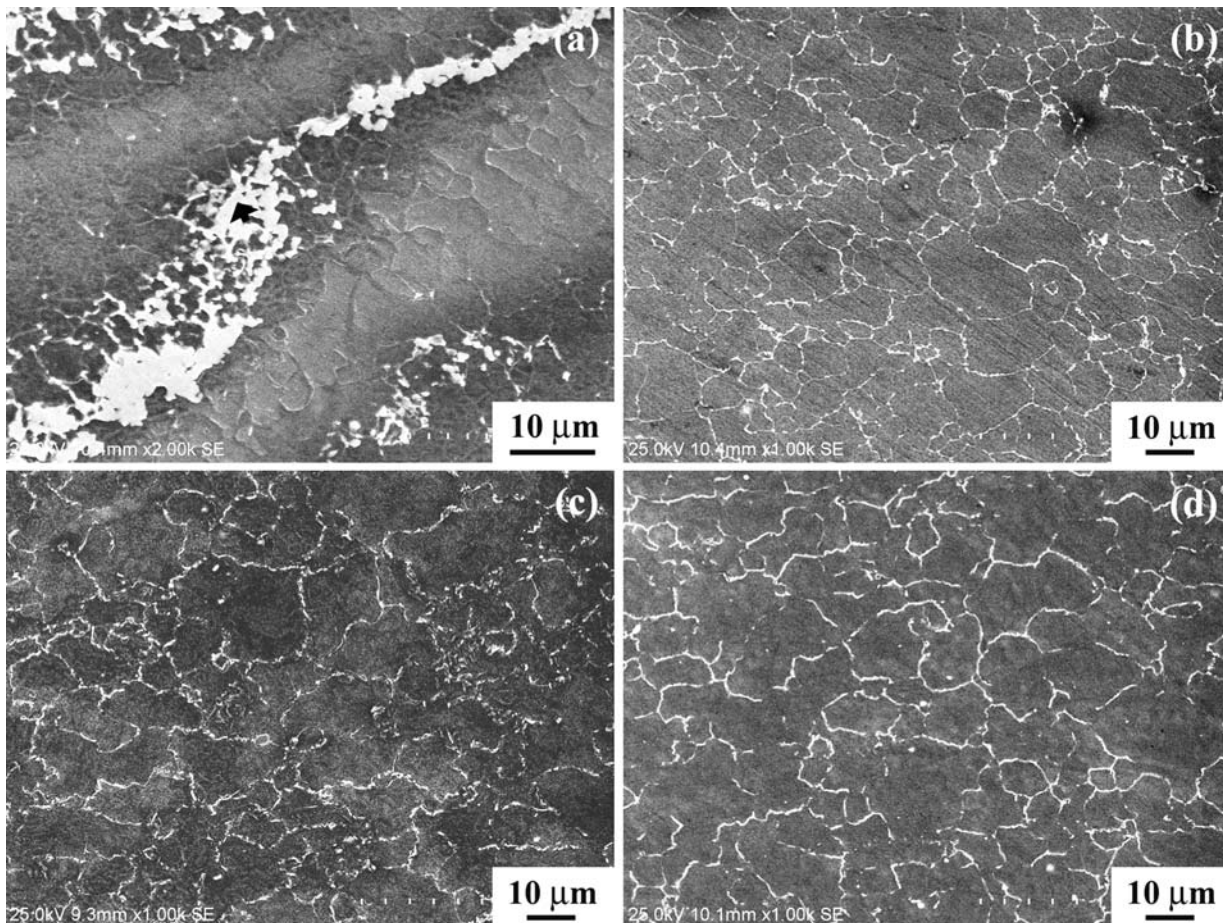


Fig. 2—SEM micrographs showing grains and  $\beta$ -Mg<sub>17</sub>Al<sub>12</sub> particle bands in SZ: (a) and (b) single-pass FSP, (c) pre-ST FSP, and (d) two-pass FSP.

**Table I. Crystal Lattice Parameter of Pre-ST and Two-Pass FSP AZ80 Samples and Pure Magnesium**

Material	<i>a</i> (Å)	<i>c</i> (Å)	<i>c/a</i>
Pre-ST FSP AZ80	3.1800	5.1734	1.626
Two-pass FSP AZ80	3.1762	5.1719	1.628
Pure Magnesium	3.2090	5.2110	1.623

The crystal lattice parameters of the as-FSP AZ80 samples tend to decrease with increasing the concentration of dissolved aluminum.

The DSC analyses indicated the presence of two endothermic peaks in the as-cast AZ80 sample (Figure 4). The first peak with the incipient temperature of 429 °C corresponds to the dissolution of the eutectic  $\beta$ -Mg<sub>17</sub>Al<sub>12</sub>

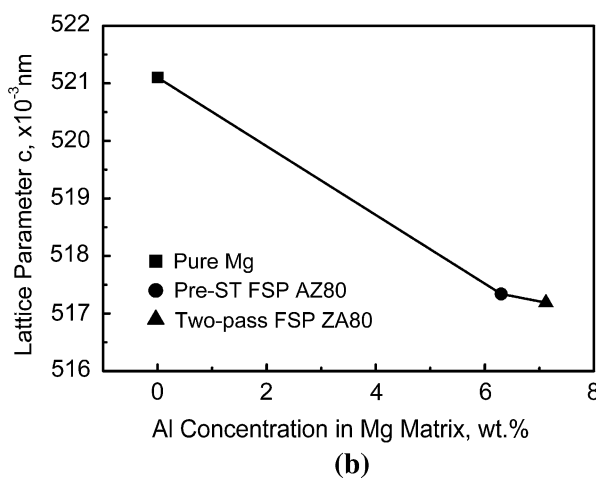
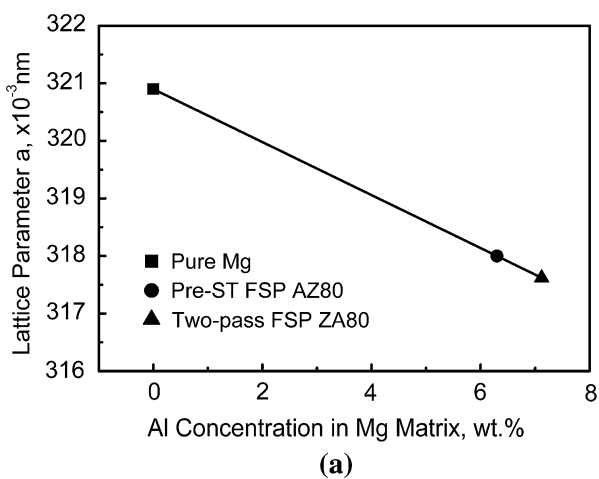


Fig. 3—Relationship between crystal lattice parameters and aluminum concentration in magnesium.

phase, whereas the second peak at higher temperature is due to the melting of the magnesium. However, for the FSP samples, the endothermic peak corresponding to the dissolution of the eutectic  $\beta$ -Mg<sub>17</sub>Al<sub>12</sub> phase disappeared. There is an exothermic peak around 250 °C and a broad endothermic peak around 370 °C in the two-pass FSP

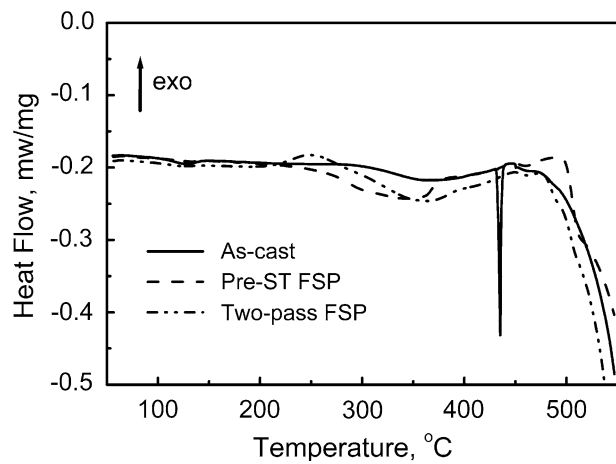


Fig. 4—DSC curves of AZ80 samples.

sample. However, only a broad endothermic peak is observed around 340 °C in the pre-ST FSP sample.

For the pre-ST FSP sample, after aging, annealing twins were observed in the BM zone (Figures 5(a) through (c)). There are two types of precipitates in the BM zone: the discontinuous precipitation (DP) and the continuous precipitation (CP). While the DP occurred at the grain boundaries, the CP formed within the grains (Figures 5(b) and (c)). Furthermore, EDS analyses indicated that there is a concentration gradient of Al element from the grain interior (point A) to the boundary (point C) (Table II). The twin boundaries are favored sites for the precipitation of the Mg<sub>17</sub>Al<sub>12</sub> phase (Figure 5(c)). In the SZ, lamellar DP developed from the grain boundaries into the grains, and the fine CP laths formed inside the grains (Figure 5(d)).

Table II. Results of EDS Analysis of Figure 5(b) (Weight Percent)

Location	Al	Mg
A	3.71	96.29
B	5.89	94.11
C	8.99	91.01

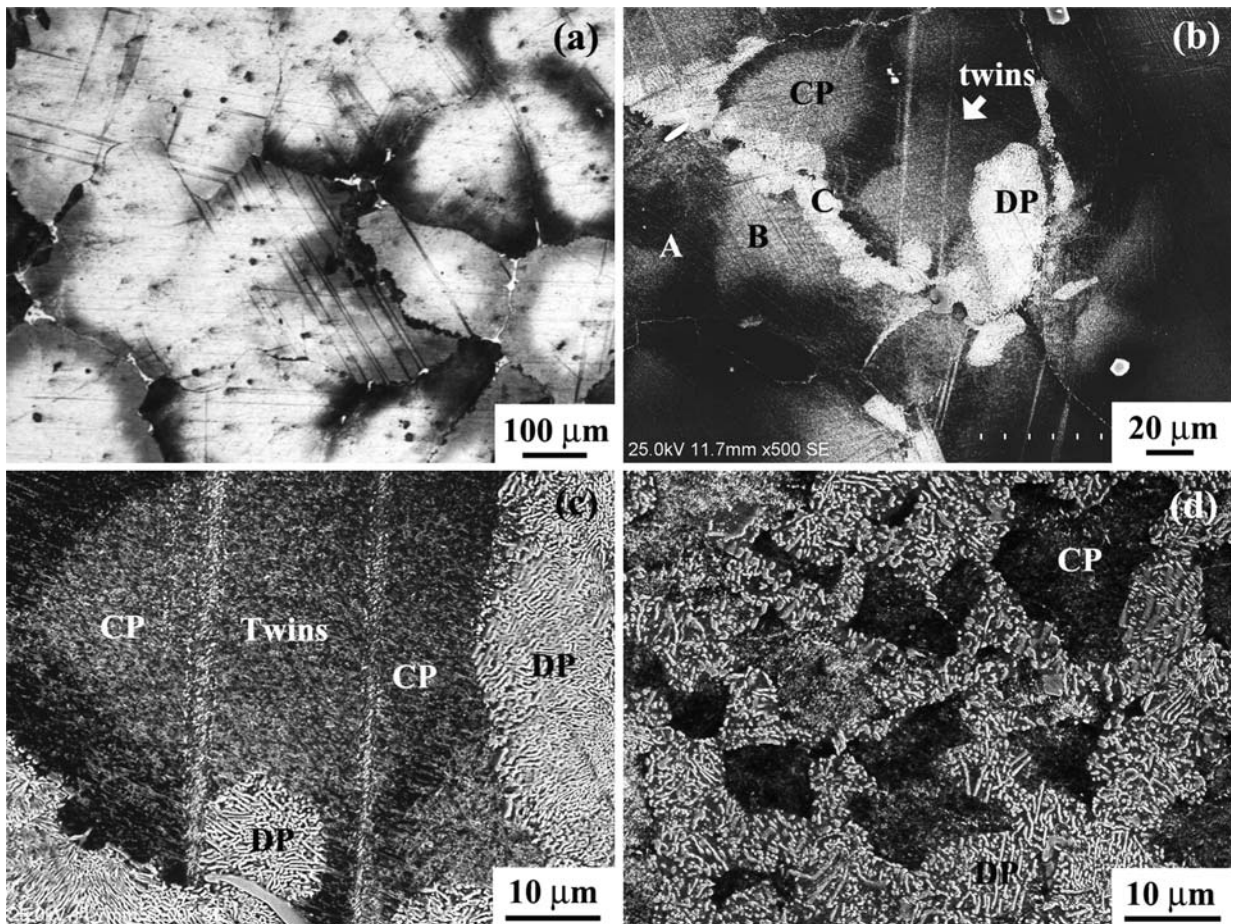


Fig. 5—Microstructure of aged pre-ST FSP AZ80 sample: (a) through (c) BM zone and (d) SZ.

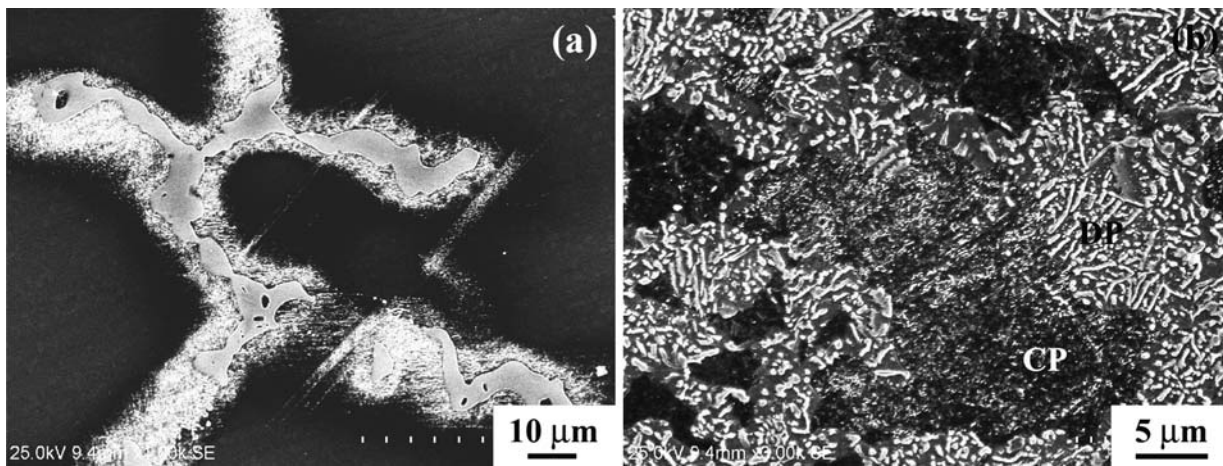


Fig. 6—Microstructure of aged two-pass FSP AZ80 sample: (a) BM zone and (b) SZ.

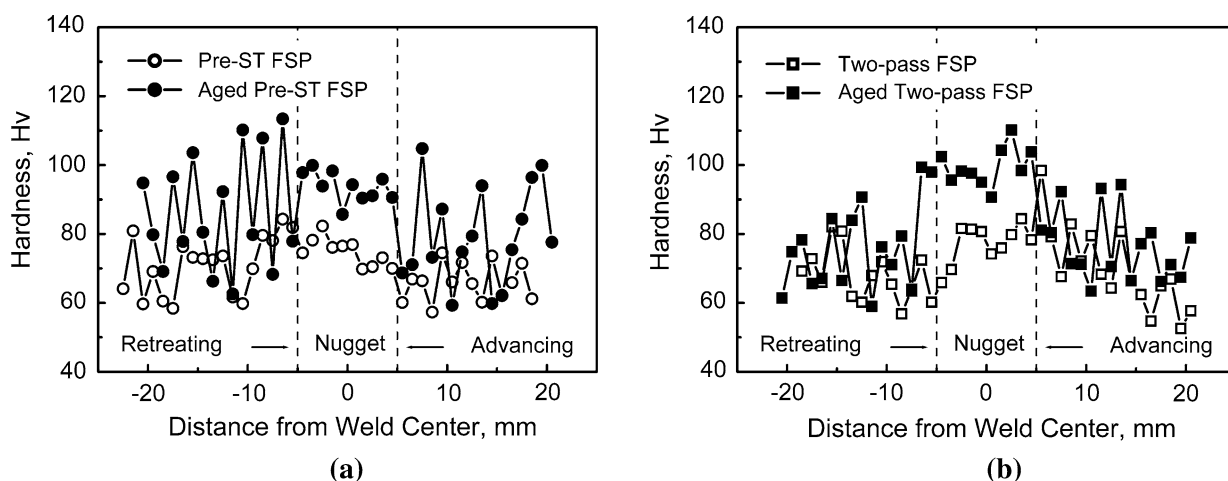


Fig. 7—Microhardness profiles of FSP AZ80 samples: (a) pre-ST FSP and (b) two-pass FSP.

For the two-pass FSP sample, aging resulted in the generation of a few  $\beta\text{-Mg}_{17}\text{Al}_{12}$  precipitates around the original coarse eutectic  $\beta\text{-Mg}_{17}\text{Al}_{12}$  network in the BM zone (Figure 6(a)). On the other hand, lamellar DP developed from the grain boundaries and extensive CP was observed within the grains in the SZ (Figure 6(b)).

For the pre-ST FSP sample, generally, the hardness of the SZ is slightly higher than that of the BM with a remarkable fluctuation (Figure 7(a)). After aging, the hardness in both BM and SZ zones increases remarkably. However, the hardness in the BM exhibits remarkable fluctuation, with the highest hardness values being higher than those of the SZ. For the two-pass FSP sample, the hardness of the SZ is higher than that of the BM with an obvious fluctuation (Figure 7(b)). After post-FSP aging, while the hardness of the BM exhibits a slight increase, the hardness of the SZ increases significantly.

Table III summarizes the room-temperature tensile properties of the cast and FSP samples. The as-received AZ80 casting exhibited lower yield strength (YS, 84 MPa), ultimate tensile strength (UTS, 121 MPa),

Table III. Tensile Properties of AZ80 Magnesium Alloy\*

Conditions	YS (MPa)	UTS (MPa)	El. (Pct)
As-cast	84.1	120.9	4.1
As-cast + solutionizing	94.3	176.5	8.8
Single-pass FSP	134.6	188.8	3.0
Aged single-pass FSP	156.5	213.3	1.2
Pre-ST FSP	109.2	308.8	25.2
Aged pre-ST FSP	169.2	336.5	16.8
Two-pass FSP	136.7	327.3	25.0
Aged two-pass FSP	192.8	355.7	17.0

\*YS: yield strength, UTS: ultimate tensile strength, and El.: elongation.

and elongation (4 pct). The single-pass FSP resulted in a significant improvement in the UTS (189 MPa) and YS (135 MPa), but a decrease in ductility (3 pct). By comparison, the pre-ST FSP sample exhibited significantly enhanced UTS (309 MPa) and ductility (25 pct) and reduced YS (109 MPa). The two-pass FSP resulted in a further enhancement in the YS and UTS (137 and

327 MPa), with a ductility being equal to that achieved in the pre-ST FSP sample. The post-FSP aging increased the strength of the FSP samples, in particular the YS, and decreased the ductility. Among the three FSP samples prepared *via* different FSP procedures, the aged two-pass FSP sample exhibited the highest UTS of 356 MPa, a YS of 193 MPa, and an elongation of 17 pct.

Figure 8 shows that the SEM fractographs of three FSP samples are quite different. For the single-pass FSP, the fracture surface was characterized by fractured  $\beta$ -Mg<sub>17</sub>Al<sub>12</sub> particles (as shown by arrows), secondary cracks, and a few cleavage planes (Figure 8(a)). This implies that the fracture initiated in the heterogeneous  $\beta$ -Mg<sub>17</sub>Al<sub>12</sub> bands and propagated in the Mg matrix. After aging, the fracture surface exhibited a shale structure that corresponded to cleavage fracture (Figure 8(b)), which was responsible for the decreased elongation (1.2 pct).

For the pre-ST FSP sample, a typical ductile dimple-fracture morphology was indicated by the dimples, short tear ribs, and a few cleavage planes (Figure 8(c)). A similar fracture surface was found in the two-pass FSP sample (Figure 8(e)). However, the dimples were more uniformly distributed and the cleavage planes were fewer than those in the pre-ST FSP sample, though almost the same elongation was observed for both FSP samples. After aging, both the pre-ST FSP and two-pass FSP samples showed flat fracture surfaces with several areas exhibiting intergranular fracture morphology (as shown by arrows) (Figures 8(d) and (f)). This indicates that the CP and DP exerted a significant effect on the deformation and fracture behavior for the FSP samples after post-FSP aging.

## IV. DISCUSSION

### A. Microstructural Characteristics

As-cast AZ alloys with higher aluminum content are generally characterized by the networklike eutectic  $\beta$ -Mg<sub>17</sub>Al<sub>12</sub> phase distributed at the grain boundaries, as shown in Figure 1(a), which results in low strength and ductility. Friction stir processing resulted in significant breakup and dissolution of the networklike eutectic  $\beta$ -Mg<sub>17</sub>Al<sub>12</sub> phase due to the stirring effect of the threaded pin and thermal exposure (Figures 1 and 2). However, the striplike structure associated with remaining Mg<sub>17</sub>Al<sub>12</sub> particle bands and heterogeneous grains was observed in the single-pass FSP AZ80 sample (Figures 1(c) and (d) and 2(a)). Similarly, the heterogeneous striplike structure was previously reported in single-pass FSP AZ91D.<sup>[16]</sup> The striplike structure, similar to the onion rings, was widely observed in the friction stir welds. The formation of the onion rings has been explained by the geometrical effect,<sup>[25]</sup> variations in grain size,<sup>[26]</sup> particle-rich bands,<sup>[27]</sup> and texture.<sup>[28]</sup> In the single-pass FSP AZ80 and AZ91D samples, the formation of the striplike structure is attributed to insufficient strain/temperature conditions due to the low tool rotation rate of 400 rpm used in this study and

Reference 16. Biallas *et al.*<sup>[29]</sup> found that the onion rings vanished when the traverse speed decreased or the rotation rate increased. This is attributed to intensified stirring and increased heat input. It is expected that when the tool rotation rate is increased, a uniform microstructure will be produced in the AZ alloy castings because intensified stirring results in more effective breakup of the coarse  $\beta$ -Mg<sub>17</sub>Al<sub>12</sub> phase and increased heat input leads to the dissolution of greater  $\beta$ -Mg<sub>17</sub>Al<sub>12</sub> phase. However, it should be pointed out that increasing the FSP heat input would result in remarkable coarsening of the recrystallized grains in the AZ magnesium alloys due to the absence of pinning particles. Therefore, increasing the heat input is not the optimum FSP procedure to homogenize the microstructure of the AZ alloy castings.

As shown in Figures 1(e) and (f) and 2(c) and (d), both the pre-ST FSP and two FSP passes improved the microstructural uniformity, resulting in the disappearance of the striplike structure. For the pre-ST FSP sample, the pre-ST resulted in the fundamental dissolution of the Mg<sub>17</sub>Al<sub>12</sub> phase and the formation of the supersaturated solid solution (Figure 1(b)). After subsequent FSP, the coarse grains in the pre-ST microstructure were converted to the fine equiaxed grains due to the occurrence of dynamic recrystallization (Figures 1(e) and 2(c)). For the two-pass FSP sample, the second FSP pass resulted in further breakup and dissolution of the remaining  $\beta$ -Mg<sub>17</sub>Al<sub>12</sub> phase particles and homogenization of the grain microstructure in the single-pass FSP sample, thereby producing a uniform microstructure with most of the aluminum being dissolved into the magnesium matrix (Figures 1(f) and 2(d)).

According to the binary phase diagram of the Mg-Al alloy, the equilibrium concentration of aluminum in magnesium at room temperature is about 1.5 wt pct. The aluminum content in the grain interior was determined by EDS to be 6.2, 6.3, and 7.1 wt pct for the single-pass, pre-ST, and two-pass FSP samples, respectively. This indicates that most of the Mg<sub>17</sub>Al<sub>12</sub> phase was dissolved into the magnesium matrix during FSP. The atom radius of aluminum (0.14 nm) is smaller than that of magnesium (0.16 nm). The dissolution of aluminum into the magnesium matrix will result in a shrinkage in the crystal lattice parameters of the magnesium solid solution. Therefore, the crystal lattice parameters in the FSP AZ80 samples, as shown in Table I, further proved that FSP resulted in the dissolution of most of the Mg<sub>17</sub>Al<sub>12</sub> phase. Figure 3 clearly shows that the crystal lattice parameters of the as-FSP AZ80 samples decreased when the concentration of dissolved aluminum was increased.

Furthermore, the disappearance of the endothermic peak in the FSP samples, corresponding to the dissolution of the eutectic  $\beta$ -Mg<sub>17</sub>Al<sub>12</sub> phase, demonstrated that most of the coarse  $\beta$ -Mg<sub>17</sub>Al<sub>12</sub> phase was dissolved during FSP (Figure 4). The exothermic peak around 250 °C and the endothermic peak around 370 °C in the two-pass FSP sample are attributed to the precipitation and dissolution of the fine  $\beta$ -Mg<sub>17</sub>Al<sub>12</sub> particles, respectively. A similar phenomenon has been reported in the

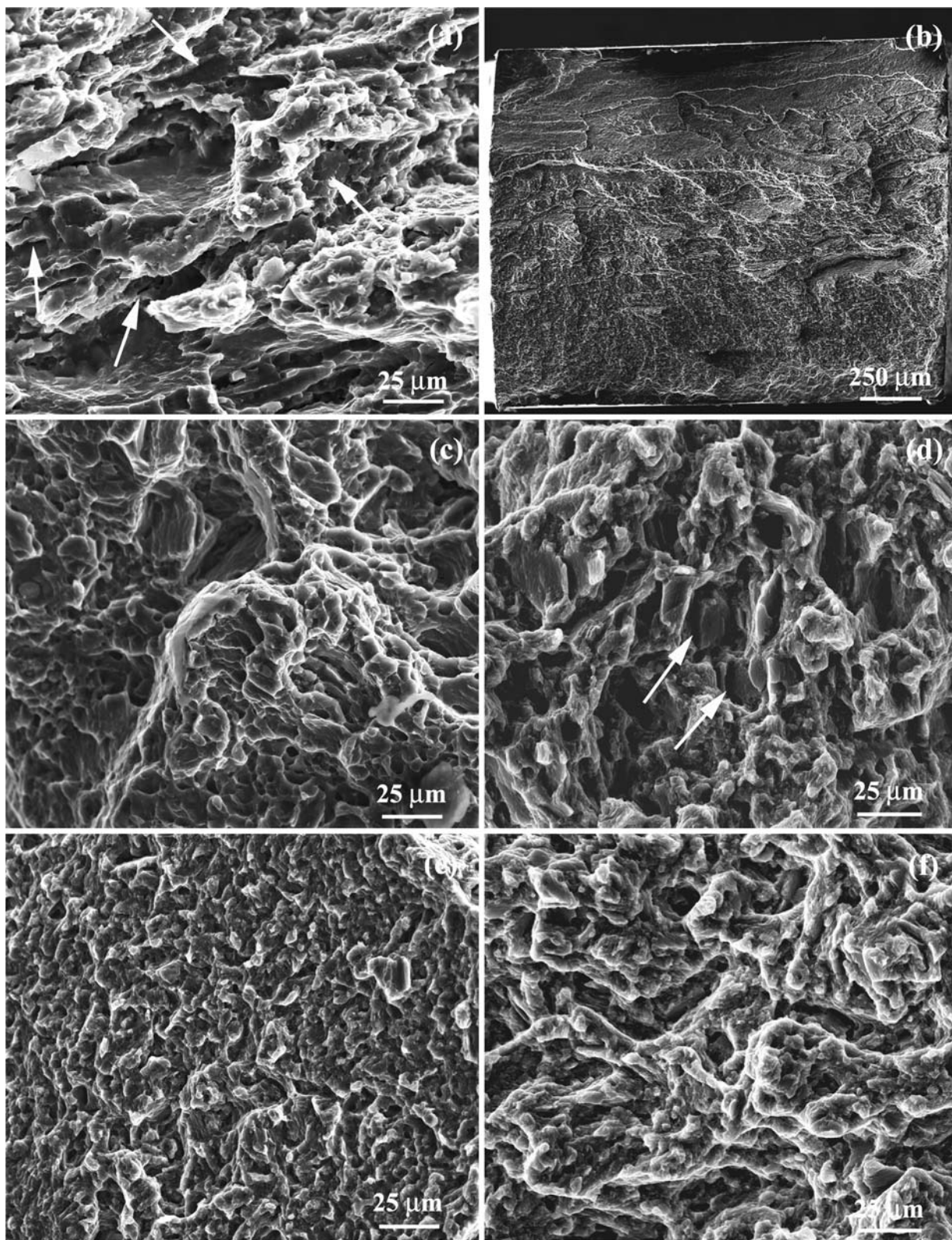


Fig. 8—SEM fractographs of FSP AZ80 samples: (a) single FSP, (b) single FSP + aging, (c) pre-ST FSP, (d) pre-ST FSP + aging, (e) two-pass FSP, and (f) two-pass FSP + aging.

two-pass FSP AZ91D magnesium alloy.<sup>[18]</sup> It was reported that the two-pass FSP on the cast AZ91D sample produced a fine-grained structure of  $\sim 15 \mu\text{m}$ ,

with 89 pct of aluminum being dissolved into the magnesium matrix.<sup>[18]</sup> These results indicate that FSP functions like a solutionizing treatment. Two-pass FSP

not only results in significant grain refinement, but also produces an effect similar to the conventional T6-solution heat treatment for the cast AZ magnesium alloys with higher aluminum content.

For cast AZ91 and AZ80, it takes up to ~40 hours to achieve the complete dissolution of the coarse eutectic  $\beta$ -Mg<sub>17</sub>Al<sub>12</sub> phase due to the low diffusion rate of aluminum in the magnesium matrix.<sup>[8]</sup> Now, the FSW/FSP thermal cycles are very short due to fast heating and cooling rates. For example, the duration the temperature remains above 200 °C during FSP of A356 aluminum alloy is only 25 seconds.<sup>[30]</sup> Therefore, the dissolution of the eutectic  $\beta$ -Mg<sub>17</sub>Al<sub>12</sub> phase in such a short period is associated with severe plastic deformation, with a strain rate of 10<sup>0</sup> to 10<sup>2</sup> s<sup>-1</sup> and strains of up to ~40.<sup>[3,31,32]</sup> A previous analysis has indicated that such a severe plastic deformation facilitates the dissolution of the  $\beta$ -Mg<sub>17</sub>Al<sub>12</sub> phase significantly, due to significantly accelerated diffusion rate and shortened diffusion distance.<sup>[16]</sup>

After a post-FSP aging at 177 °C for 10 hours, fine  $\beta$ -Mg<sub>17</sub>Al<sub>12</sub> particles precipitated from the supersaturated solid solution in the forms of DP and CP for both pre-ST and two-pass FSP AZ80 samples, as shown in Figures 5(d) and 6(b). The DP, also known as cellular precipitation because the composition of the matrix changes discontinuously as the cell front passes, developed from the grain boundaries,<sup>[33]</sup> whereas the CP formed within the grains with five types of orientation relationships between the Mg<sub>17</sub>Al<sub>12</sub> phase plates and magnesium matrix.<sup>[34]</sup> In the aged BM sample with the pre-ST, the obvious concentration gradient of Al element from the grain interior to its boundary (Table II) indicates that although the pre-ST at 415 °C for 16 hours dissolved most of the Mg<sub>17</sub>Al<sub>12</sub> phase into the magnesium matrix, the solute distribution in the matrix was not uniform. This implies that a longer solution time is needed to homogenize the microstructure of AZ alloy castings. Furthermore, the annealing twins were observed in the aged BM with the pre-ST. Such twins are often observed in annealed coarse magnesium alloys<sup>[35]</sup> and believed to favor the precipitation of the Mg<sub>17</sub>Al<sub>12</sub> phase particles.<sup>[36]</sup> The precipitation of a few  $\beta$ -Mg<sub>17</sub>Al<sub>12</sub> around the original coarse eutectic  $\beta$ -Mg<sub>17</sub>Al<sub>12</sub> network in the aged as-cast BM sample (Figure 6(a)) is due to the fact that the magnesium matrix of the as-cast AZ alloys is usually a little supersaturated.<sup>[18]</sup>

## B. Hardness and Tensile Properties

For the pre-ST FSP sample, significant grain refinement in the SZ made the hardness of the SZ higher than that of the BM zone (Figure 7(a)). After post-FSP aging, the precipitation of the fine Mg<sub>17</sub>Al<sub>12</sub> particles significantly increased the hardness of both BM and SZ. The hardness fluctuation of the BM under both as-solutionized and aged conditions is associated with the obvious concentration gradient of Al element from the grain interior to the boundaries (Table II). Especially, under aged condition, the BM zone exhibited remarkable hardness fluctuation, with the highest hardness values

being higher than those of the SZ due to high density of the precipitates at the grain boundaries, as shown in Figure 5(b).

For the two-pass FSP sample, FSP resulted in significant grain refinement and the breakage and dissolution of most of the coarse  $\beta$ -Mg<sub>17</sub>Al<sub>12</sub> phase in the AZ80 casting, thereby increasing the hardness of the SZ. Therefore, the hardness of the SZ is higher than that of the BM (Figure 7(b)). The post-FSP aging resulted in the precipitation of fine Mg<sub>17</sub>Al<sub>12</sub> particles in continuous and discontinuous forms in the SZ (Figure 6(b)), thereby increasing the hardness of the SZ significantly. However, aged BM zone did not exhibit an obvious hardness increase due to limited precipitation of the fine  $\beta$ -Mg<sub>17</sub>Al<sub>12</sub> particles around the original coarse eutectic  $\beta$ -Mg<sub>17</sub>Al<sub>12</sub> network (Figure 6(a)). Therefore, after aging, the hardness of the SZ is substantially higher than that of the BM zone (Figure 7(b)). The marked hardness fluctuation of the BM zone under as-cast and aged conditions is attributed to the presence of coarse  $\beta$ -Mg<sub>17</sub>Al<sub>12</sub> phase.

The as-received AZ80 magnesium alloy exhibited lower YS and UTS (84 and 121 MPa) and elongation (4 pct) (Table I). This is attributed to the presence of a coarse eutectic  $\beta$ -Mg<sub>17</sub>Al<sub>12</sub> network at the grain boundaries that tends to crack or debond from the magnesium matrix early under lower stress during tensile deformation.<sup>[18]</sup> Similar fracture characteristics have been previously observed in a cast AZ91 alloy.<sup>[37]</sup>

The single-pass FSP sample exhibited an enhancement in both YS and UTS with a reduced ductility. This is attributed to the insufficient dissolution of the coarse  $\beta$ -Mg<sub>17</sub>Al<sub>12</sub> phase and heterogeneous microstructure, indicating that the distribution and morphology of the  $\beta$ -Mg<sub>17</sub>Al<sub>12</sub> phase play an important role in determining the mechanical properties. Many fractured  $\beta$ -Mg<sub>17</sub>Al<sub>12</sub> particles and the secondary cracks in the fracture surfaces of the single-pass FSP sample (Figure 8(a)) indicate that the crack initiated in the  $\beta$ -Mg<sub>17</sub>Al<sub>12</sub> bands (Figure 2(a)). The crack propagated along the bands and eventually into the Mg matrix, resulting in the cleavage planes. It is well known that microcracks develop along (0002) crystal planes for Mg alloys. For the FSP Mg alloys, the (0002) plane is roughly distributed along the tool rotation direction,<sup>[4]</sup> which corresponds with the  $\beta$ -Mg<sub>17</sub>Al<sub>12</sub> bands. Thus, the crack propagated easily from the intermetallic bands into the Mg grains, leading to low ductility.

Both the pre-ST FSP and two FSP passes resulted in a significant improvement in YS and UTS, particularly ductility due to significant breakup and dissolution of the coarse eutectic  $\beta$ -Mg<sub>17</sub>Al<sub>12</sub> phase, homogeneous microstructure, and remarkable grain refinement. The tensile properties of the two-pass FSP sample were slightly higher than those of the pre-ST FSP sample. The enhancement in the strength of the two-pass FSP sample was attributed to the finer grains and the higher aluminum concentration in magnesium. It is noted that the two-pass FSP sample exhibited fewer cleavage planes and more uniformly distributed dimples in the fracture surface than the pre-ST FSP sample (Figures 8(c) and (e)), indicating a more uniform deformation due to finer grains and lower  $\beta$ -Mg<sub>17</sub>Al<sub>12</sub> content.

A post-FSP aging resulted in a significant increase in YS and UTS and a decrease in the ductility in the FSP AZ80 samples due to the precipitation of the fine  $\beta$ -Mg<sub>17</sub>Al<sub>12</sub> phase particles. The lowest elongation of the single-FSP sample can be easily related to the brittle feature of the fracture surface (Figure 8(b)). The precipitated cellular  $\beta$ -Mg<sub>17</sub>Al<sub>12</sub> promoted the propagation of cracks, which initiated in the heterogeneous intermetallic bands (Figure 2(a)). For the pre-ST FSP and two-pass FSP samples, the intergranular fracture and flat fracture surface (Figures 8(d) and (f)) indicate that the crack initiated and propagated in the DP along the grain boundaries and the CP in the grains. Therefore, the elongation for both FSP samples decreased, although YS and UTS increased by the fine  $\beta$ -Mg<sub>17</sub>Al<sub>12</sub> phase particles. The aged two-pass FSP sample exhibited the highest YS and UTS, which is attributed to the finer grains and the precipitation of more fine  $\beta$ -Mg<sub>17</sub>Al<sub>12</sub> particles resulting from higher dissolved aluminum concentration.

## V. CONCLUSIONS

1. Friction stir processing not only resulted in significant grain refinement, but also produced an effect similar to the conventional T6-solution treatment for the cast AZ80 magnesium alloy. Most of the coarse networklike Mg<sub>17</sub>Al<sub>12</sub> phase in the as-cast alloy was dissolved into the magnesium matrix during FSP, thereby forming a supersaturated solid solution.
2. While a heterogeneous microstructure with the Mg<sub>17</sub>Al<sub>12</sub> particle-rich bands was observed in the single FSP sample, both the pre-ST prior to FSP and second FSP pass resulted in the generation of a uniform microstructure.
3. Compared to the as-cast AZ80 sample, the single FSP sample exhibited increased strength and reduced ductility. The reduced ductility was attributed to the heterogeneous microstructure. By comparison, the pre-ST and two-pass FSP samples exhibited significantly enhanced strength and ductility.
4. Among the three FSP procedures, the aged two-pass FSP sample exhibited the highest UTS of 356 MPa and an elongation of 17 pct.

## ACKNOWLEDGMENTS

The authors gratefully acknowledge the support of (a) the National Outstanding Young Scientist Foundation of China under Grant No. 50525103, (b) the National Basic Research Program of China under Grant No. 2006CB605205, (c) the Hundred Talents Program of Chinese Academy of Sciences, (d) the National High-tech Research Program under Grant No. 2006AA03Z111, and (e) the China Postdoctoral Science Foundation for A.H. Feng.

## REFERENCES

1. B.L. Mordike and T. Ebert: *Mater. Sci. Eng. A*, 2001, vol. 302, pp. 37–45.
2. *ASM Speciality Handbook, Magnesium and Magnesium Alloys*, ASM INTERNATIONAL, Materials Park, OH, 1999, pp. 1–314.
3. C.I. Chang, C.J. Lee, and J.C. Huang: *Scripta Mater.*, 2004, vol. 51, pp. 509–14.
4. Y.N. Wang, C.I. Chang, C.J. Lee, H.K. Lin, and J.C. Huang: *Scripta Mater.*, 2006, vol. 55, pp. 637–40.
5. F. Khomamizadeh, B. Nami, and S. Khoshkhouei: *Metall. Mater. Trans. A*, 2005, vol. 36A, pp. 3489–94.
6. S.J. Guo, Q.C. Le, Z.H. Zhao, Z.J. Wang, and J.Z. Cui: *Mater. Sci. Eng. A*, 2005, vol. 404, pp. 323–29.
7. D.H. Stjohm, M. Qian, M.A. Easton, P. Cao, and Z. Hildebrand: *Metall. Mater. Trans. A*, 2005, vol. 36A, pp. 1669–79.
8. S. Kleiner, O. Beffort, and P.J. Uggowitzer: *Scripta Mater.*, 2004, vol. 51, pp. 405–10.
9. Y. Wang, G. Liu, and Z. Fan: *Scripta Mater.*, 2006, vol. 54, pp. 903–08.
10. K. Máthis, J. Gubicza, and N.H. Nam: *J. Alloys Compd.*, 2005, vol. 394, pp. 194–99.
11. W.M. Thomas, E.D. Nicholas, J.C. Needham, M.G. Murch, P. Templesmith, and C.J. Dawes: G.B. Patent Application No. 9125978.8, Dec. 1991.
12. R.S. Mishra and Z.Y. Ma: *Mater. Sci. Eng. R*, 2005, vol. 50, pp. 1–78.
13. R.S. Mishra, M.W. Mahoney, S.X. McFadden, N.A. Mara, and A.K. Mukherjee: *Scripta Mater.*, 2000, vol. 42, pp. 163–68.
14. Z.Y. Ma and R.S. Mishra: *Scripta Mater.*, 2005, vol. 53, pp. 75–80.
15. R.S. Mishra, Z.Y. Ma, and I. Charit: *Mater. Sci. Eng. A*, 2003, vol. 341, pp. 307–10.
16. Z.Y. Ma, A.L. Pilchak, M.C. Juhas, and J.C. Williams: *Scripta Mater.*, 2008, vol. 58, pp. 361–66.
17. Z.Y. Ma: *Metall. Mater. Trans. A*, 2008, vol. 39A, pp. 642–58.
18. A.H. Feng and Z.Y. Ma: *Scripta Mater.*, 2007, vol. 56, pp. 397–400.
19. F.Y. Hung, C.C. Shih, L.H. Chen, and T.S. Lui: *J. Alloys Compd.*, 2007, vol. 428, pp. 106–14.
20. C.J. Lee, J.C. Huang, and X.H. Du: *Scripta Mater.*, 2007, vol. 56, pp. 875–78.
21. B.M. Darras, M.K. Khraisheh, F.K.A. Farha, and M.A. Omar: *J. Mater. Proc. Technol.*, 2007, vol. 191, pp. 77–81.
22. C.I. Chang, X.H. Du, and J.C. Huang: *Scripta Mater.*, 2007, vol. 57, pp. 209–12.
23. W. Woo, H. Choo, D.W. Brown, P.K. Liaw, and Z. Feng: *Scripta Mater.*, 2006, vol. 54, pp. 1859–64.
24. P. Cavaliere and P.P. De Marco: *J. Mater. Proc. Technol.*, 2007, vol. 184, pp. 77–83.
25. K.N. Krishnan: *Mater. Sci. Eng. A*, 2002, vol. A327, pp. 246–51.
26. J.A. Schneider and A.C. Nunes: *Metall. Mater. Trans. B*, 2004, vol. 35B, pp. 777–83.
27. M.A. Sutton, B. Yang, A.P. Reynolds, and R. Taylor: *Mater. Sci. Eng. A*, 2002, vol. A323, pp. 160–66.
28. S.W. Xu and X.M. Deng: *Acta Mater.*, 2008, vol. 56, pp. 1326–41.
29. G. Biallas, R. Braun, C.D. Donne, G. Staniek, and W.A. Kaysser: *Proc. 1st Int. Symp. on Friction Stir Welding*, Thousand Oaks, CA, June 1999.
30. Z.Y. Ma, S.R. Sharma, and R.S. Mishra: *Metall. Mater. Trans. A*, 2006, vol. 37A, pp. 3323–36.
31. K. Masaki, Y.S. Sato, M. Maeda, and H. Kokawa: *Scripta Mater.*, 2008, vol. 58, pp. 355–58.
32. P. Heurtier, C. Desrayaud, and F. Montheillet: *Mater. Sci. Forum*, 2002, vols. 396–402, pp. 1537–42.
33. D.A. Porter and K.E. Easterling: *Phase Transformations in Metals and Alloys*, University of Lulea, New York, NY, 1981, pp. 1–446.
34. S. Celotto: *Acta Mater.*, 2000, vol. 48, pp. 1775–87.
35. O. Sitdikov, R. Kaibyshev, and T. Sakai: *Mater. Sci. Forum*, 2003, vols. 419–422, pp. 521–26.
36. J.B. Clark: *Acta Metall.*, 1968, vol. 16, pp. 141–52.
37. Y.Z. Lü, Q.D. Wang, W.J. Ding, X.Q. Zeng, and Y.P. Zhu: *Mater. Lett.*, 2000, vol. 44, pp. 265–68.